Exsolution textures of orthopyroxene and clinopyroxene in high-grade BIF of the Voronezh Crystalline Massif: evidence of ultrahigh-temperature metamorphism

V. I. FONAREV[1], S. M. PILUGIN[2], K. A. SAVKO[2] AND M. A. NOVIKOVA[2]

[1]*Institute of Experimental Mineralogy, Russian Academy of Sciences, Chernogolovka, 142432, Russia (fonarev@iem.ac.ru)*
[2]*Voronezh State University, Voronezh, 394006, Russia*

ABSTRACT   Archaean banded iron formation (BIF) of the Voronezh Crystalline Massif (VCM) contains coexisting clino- and orthopyroxenes with exsolution textures. The pyroxene in the VCM BIF is found in two generations, with only the first generation containing such textures. Clinopyroxene contains large (up to 5–10 μm) (0 0 1) orthopyroxene (Opx1L) lamellae in a host clinopyroxene (Cpx1H). This host Cpx, in turn, exsolves into thin ($\sim$1 μm) (1 0 0) lamellae of orthopyroxene (Opx2L) and clinopyroxene (Cpx2H). Orthopyroxene exhibits similar exsolution textures with large (up to 50 μm) (0 0 1) clinopyroxene (Cpx1L) lamellae developed in a host orthopyroxene (Opx1H). This clinopyroxene Cpx1L shows further exsolution of thin (1 0 0) Opx2LL lamellae and clinopyroxene (Cpx2LH). Point microprobe analysis, raster-mode microprobe analysis, and microprobe element mapping of mineral grains with a large number of point analysis were used to determine the composition of the exsolution products and the primary chemistry of the coexisting clinopyroxene (CaO = 14.86–17.26 wt%) and pigeonite (CaO = 4.45–6.23 wt%). These pyroxenes crystallized during the peak of metamorphism, and application of the Lindsley geothermometer suggested that they formed at extremely high temperatures of about 1000 °C. Primary very dense CO_2-rich fluid inclusions (ρ = 1.152 g cm^{-3}, T_h = −49.2 °C) were discovered for the first time in these BIF. With these data, the metamorphic pressure was estimated as 10–11 kbar (depth 36–40 km). Such ultrahigh temperature–high pressure (UHT–HP) conditions for the regional metamorphism of the Precambrian BIF have previously been reported only for Archaean meta-ironstone from the Napier Complex (Enderby Land, Antarctica). They give an insight into the peak metamorphic conditions of the BIF of the VCM, their burial under thickened continental crust during this period of Earth evolution and suggest a more complicated multistage metamorphic and tectono-thermal history for the region than has previously been postulated.

Key words: Archaean BIF; clino–orthopyroxene; exsolution; UHT-HP metamorphism.

INTRODUCTION

Precambrian banded iron formations (BIF) are an inherent constituent of ancient shield metasedimentary rocks which mainly developed in the Archaean and Proterozoic. They are dominated by magnetite quartzites, and the relatively simple mineralogy and chemistry make them useful indicators of the physicochemical metamorphic conditions (T, P, f_{O_2}, P_{H_2O} & P_{CO_2}) and, hence, of the early tectono-thermal and geodynamic history of the Earth. Precambrian BIF are widespread in the Voronezh Crystalline Massif (VCM). This massif, along with the Ukrainian Shield (Fig. 1a,b), is one of the three crystalline segments (Fennoscandia, Volgo-Uralia and Sarmatia) of the East European craton (Gorbatschev & Bogdanova, 1993; Bogdanova *et al.*, 1996). The VCM (about 600 × 800 km in size) forms the north-eastern part of Sarmatia which was separated from the Ukrainian Shield by the Dniepr-Donets aulacogen in the Phan-

erozoic. In the east, the Lipetsk-Losev Volcanic Belt and the East Voronezh turbidite-schist province follow the boundary between the VCM and the Volgo-Uralian crustal segments (Fig. 1b,c). According to absolute age data available (see Shchipansky & Bogdanova, 1996), various MesoArchaean to latest NeoArchaean and Palaeoproterozoic terranes are present in the VCM, but distinctions between them as well as their geological boundaries, especially in the case of prograde and retrograde Archaean rocks, are still conjectural. Archaean high-grade basement rocks are preserved as relics (crustal blocks) in the migmatites and gneisses of the undivided Archaean–Palaeoproterozoic Oboyan Supergroup (Fig. 1c,d) developed in the central part of the VCM (Oskol domain) and metamorphosed predominantly in the retrograde amphibolite facies. High-grade rocks are dominated by alternating layers (from 1–2 to 30–35 m thick) of magnetite quartzites, metaultrabasites, metagabbroids and metapelites. This complex is marked by intense
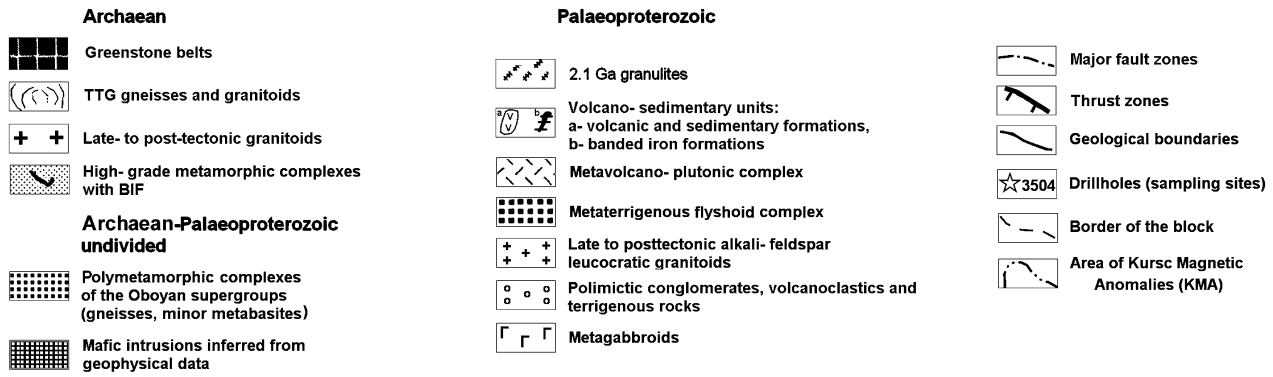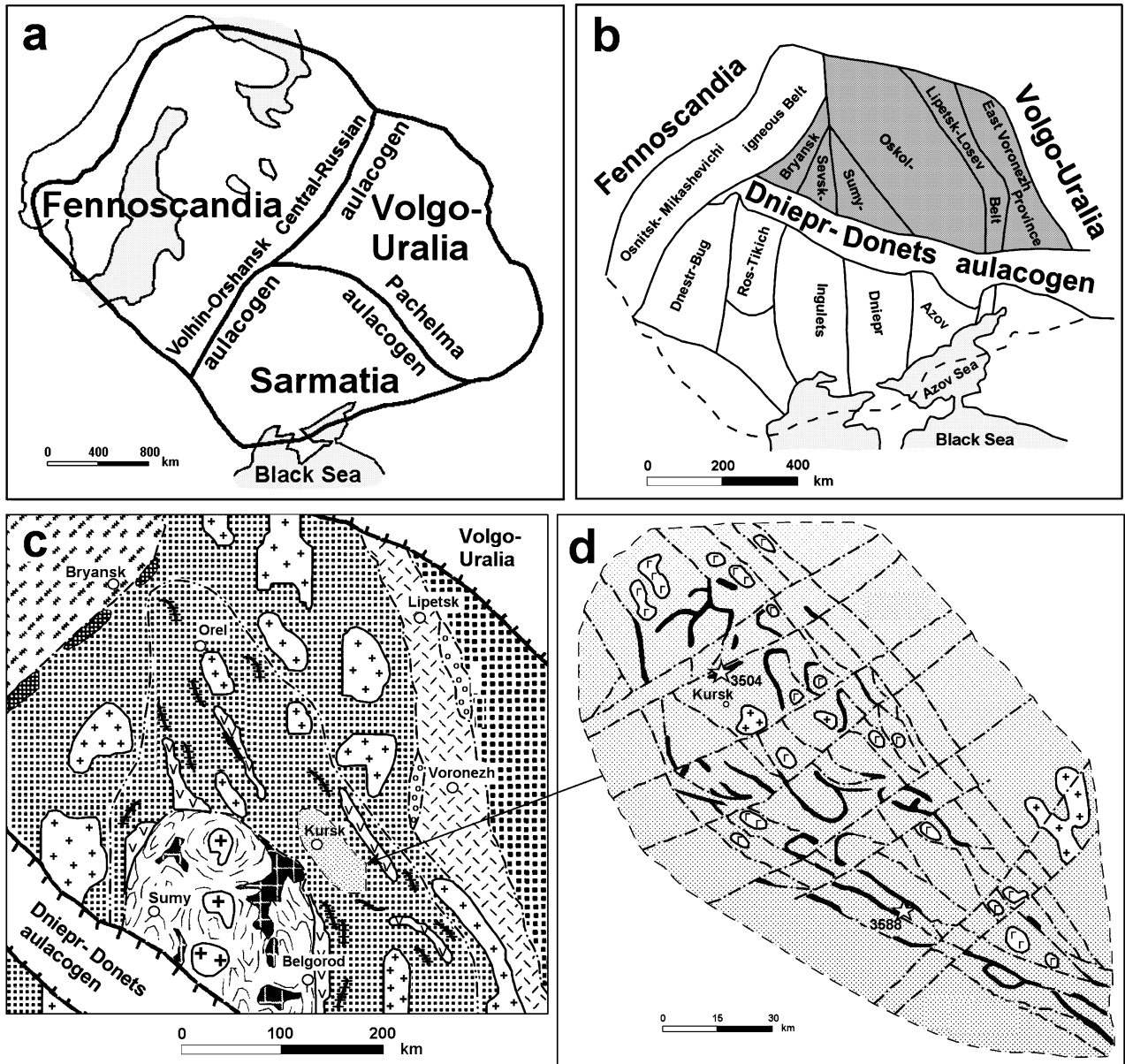
Archaean

Greenstone belts

TTG gneisses and granitoids

+ + **Late- to post-tectonic granitoids**

**High- grade metamorphic complexes
with BIF**

**Archaean-Palaeoproterozoic
undivided**

**Polymetamorphic complexes
of the Oboyan supergroups
(gneisses, minor metabasites)**

**Mafic intrusions inferred from
geophysical data**

Palaeoproterozoic

2.1 Ga granulites

**Volcano- sedimentary units:
a- volcanic and sedimentary formations,
b- banded iron formations**

Metavolcano- plutonic complex

Metaterrigenous flyshoid complex

**Late to posttectonic alkali- feldspar
leucocratic granitoids**

**Polimictic conglomerates, volcanoclastics and
terrigenous rocks**

Metagabbroids

Major fault zones

Thrust zones

Geological boundaries

☆3504 Drillholes (sampling sites)

Border of the block

**Area of Kursc Magnetic
Anomalies (KMA)**

Fig. 1. (a) Three-segment subdivision of the East European Craton (Gorbatschev & Bogdanova, 1993). (b) Crustal domains in the Sarmatian crustal segment (Shchipansky & Bogdanova, 1996). The Voronezh crystalline massif is shown by dark grey colour. (c) Simplified geological sketch map of the Voronezh crystalline massif (after Shchipansky & Bogdanova, 1996, with some changes). (d) Crustal block of Archaean high-grade rocks in the central part of Voronezh crystalline massif (sampling area).

magnetic anomalies and was studied by 100–800 m deep drill holes. Palaeoproterozoic rocks fill narrow linear zones of intracontinental rifts. BIF are present both in Archaean and in Palaeoproterozoic terranes. The Archaean BIF rocks are relatively scarce and occur as elongated bodies (positive magnetic anomalies) up to 10 km long and no more than 100 m wide. The most widespread BIF are of Palaeoproterozoic age and belong to the Kursk Group. They are marked by intense magnetic anomalies [such as the Kursk Magnetic Anomaly (KMA)]. The Archaean age of the BIF studied (Fig. 1d) is confirmed by Pb^{207}/Pb^{206} zircon geochronology of 3178 ± 39 Ma (Artemenko, 1995) from a plagiogranite dyke which cuts granulite rocks with BIF (drill hole no. 3588, depth 262.5–265.8 m). This value can also be considered as the upper age limit of the metamorphism.

There is little quantitative information on the conditions of metamorphism of the granulite complexes of the VCM (Savko, 1999a,b, 2000). An unusual feature of these granulite complexes is the development of exsolution textures in the ortho- and clinopyroxenes of the magnetite quartzites, that was originally found in the hypersthene only (Savko, 1999a). Such exsolution in pyroxene appears to be very rare in BIF (magnetite quartzites), as we know of only three other localities where such textures have been documented. One is the Biwabik Iron Formation in Minnesota (Bonnichsen, 1969), which is contact-metamorphosed by the Duluth intrusive complex. A second locality is the Stillwater Iron Formation in Montana, which was metamorphosed to > 800 °C and 2 kbar in the contact aureole of the Stillwater intrusive complex (Vaniman *et al.*, 1980). The third locality consists of Archaean high-Fe rocks (BIF) of the Napier Complex, Enderby Land, Antarctica (Sandiford & Powell, 1986; Harley, 1987). Exsolution textures in metamorphic pyroxene were examined using the experimental data of Lindsley (1983) from which ultrahigh temperatures (UHT) (980–1020 °C) of pyroxene (including pigeonite) crystallization and of the regional metamorphism in the Napier Complex were established (Harley, 1987). Unfortunately, corresponding data about the metamorphic pressures of the BIF with such pyroxenes were not obtained.

The evaluation of the peak *P–T* metamorphic conditions of the Mesoarchaean BIF of the VCM was the main task of this study. Such evaluation became possible after the detection and detailed investigation of metamorphic ortho- and clinopyroxenes with exsolution texture and high-density fluid inclusions in these rocks. Such pyroxenes and fluid inclusions are rather rare for high-grade parametamorphic rocks. The obtained data can be comparable only with the regionally metamorphosed BIF of the Napier Complex, although the similar discoveries in the other regions (e.g. on the Ukrainian shield) as well, are quite possible.

STUDY METHODS

Microprobe analyses of coexisting minerals were carried out on polished thin sections following petrographic examination. A CamScan X-ray microprobe equipped with a Link EDS analytical system (Institute of Experimental Mineralogy, Russian Academy of Sciences) was used for the analyses. The operating conditions were: 20 kV accelerating voltage, 1.2 mA beam current, 70 s counting time, and a beam 1–5 μm in diameter or, sometimes, analysis in 250- to 500-μm raster mode, when it was necessary to determine the composition of minerals with exsolution lamellae. The ZAF correction in calculating the oxide concentrations and assaying the accuracy was conducted with the standard software of the system. The analytical accuracy was systematically monitored by running replicate analyses of standards of natural and synthetic minerals. From 40 to 250 spot analyses were obtained for each sample. Some representative analyses (including averaged data) are listed in Table 1. An attempt to obtain the integrated compositions of pyroxene (Table 1) was made by raster scanning, or by compositional mapping with a great number of individual spot analyses. The raster analyses often significantly varied over the area of the grain, and as shown by petrographic observation, this was caused by insufficiently full representation of exsolution products at the surface of the thin sections resulting in distortion of their actual proportions in the minerals. This caused overestimation of the Ca content in clinopyroxene and, conversely, its underestimation in orthopyroxene. Reintegration of the primary compositions of the exsolved pyroxene is a major problem. We attempted to solve it by selecting grains with the greatest amount of the visible exsolution products. Thus analyses with the lowest CaO content in clinopyroxene and highest in orthopyroxene were considered as the most likely to be representative of the integrated compositions of the primary minerals.

Fluid inclusions were studied in double-polished 200–300 μm thick sections using a Linkam heating/freezing stage with a working temperature range of −196 °C to 600 °C (THMSG 600) and an automated sample heating–cooling with rates from 0.1 to 90 °C min^{-1}, reproducible to 0.1 °C. The stage was systematically calibrated using natural CO_2 (Camperio, Alps) and synthetic (H_2O) inclusions in quartz. Changes in the inclusions were observed under an optical microscope or using a digital video camera. From three to 23 different mineral grains were studied for each sample (up to 32 fluid inclusions in each grain). The density, molar volumes and isochores of fluid inclusions were calculated using the FLUIDS 1 package (Bakker, 2003). The interpretation of the microthermometric data was based on the notion of 'groups of synchronous inclusions'

Table 1. Representative electron microprobe analyses of minerals of the BIF from the Voronezh crystalline massif.

Sample	3504-V16										
No. grain	2	4	5	5	6	8	9(4)	9(4)	1	1,2	6
Mineral	CpxI	CpxI	OpxI	OpxI	OpxI	OpxI	OpxI	OpxI	OpxI	CpxI	CpxI
No. analyses	1 (av)	2 (av)	7 (av)	8 (av)	81	5 (av)	26a	9 (av)	6 (av)	4 (av)	Av 3
Varieties	CpxP	CpxP	Opx1H	Cpx1L	Pgt	Pgt	Cpx1L	Opx1H	Pgt	Cpx1H	Opx1L
n	16 (R)	32 (Lc)	4 (Lc)	3 (Lc)	1 (R)	2 (R)	1 (R)	2 (Lc)	2 (R)	2 (R)	2 (Lc)
SiO_2	49.06	48.79	47.21	49.39	48.10	48.12	49.39	48.11	48.17	49.31	47.94
TiO_2	0.03	0.04	0.03	0.12	–	0.04	0.04	0.08	0.03	0.06	–
Al_2O_3	0.03	0.01	–	0.02	–	0.05	0.04	0.01	–	–	–
Cr_2O_3	0.15	0.07	–	–	–	0.13	–	0.01	0.13	0.01	0.02
FeO*	24.31	26.84	41.32	20.59	37.35	35.46	20.84	40.28	38.47	21.68	40.55
MnO	1.40	1.45	2.69	1.06	2.26	2.32	0.97	2.34	2.27	1.19	3.34
MgO	7.36	7.49	8.14	7.13	8.07	7.86	7.32	8.29	8.16	7.32	7.41
CaO	17.24	14.82	0.74	21.05	4.46	6.23	20.52	0.84	3.06	19.66	0.79
Na_2O	0.27	0.20	–	0.30	–	0.09	0.47	0.08	0.07	0.33	0.05
K_2O	0.01	–	0.02	–	–	–	–	0.06	0.01	–	0.03
Total	99.86	99.71	100.15	99.66	100.24	100.30	99.59	100.10	100.37	99.56	100.13
Si	1.97	1.97	1.96	1.97	1.98	1.97	1.97	1.99	1.98	1.97	1.99
Al^{IV}	–	–	–	–	–	–	–	–	–	–	–
Ti	–	–	–	–	–	–	–	–	–	–	–
Cr	0.01	–	–	–	–	0.01	–	–	0.01	–	–
Fe^{2+}	0.82	0.91	1.44	0.69	1.28	1.21	0.70	1.39	1.32	0.73	1.41
Mn	0.05	0.05	0.10	0.04	0.08	0.08	0.03	0.08	0.08	0.04	0.12
Mg	0.44	0.45	0.51	0.42	0.49	0.48	0.44	0.51	0.50	0.44	0.46
Ca	0.74	0.64	0.03	0.90	0.20	0.27	0.88	0.04	0.14	0.84	0.04
Na	0.02	0.02	–	0.02	–	0.01	0.04	0.01	0.01	0.03	0.01
K	–	–	–	–	–	–	–	–	–	–	–
T Site	1.97	1.97	1.96	1.97	1.98	1.97	1.97	1.99	1.98	1.97	1.99
O Site	2.07	2.07	2.07	2.07	2.05	2.06	2.08	2.03	2.05	2.07	2.02
All	4.04	4.04	4.04	4.04	4.03	4.03	4.05	4.02	4.02	4.04	4.01
O	6.00	6.00	6.00	6.00	6.00	6.00	6.00	6.00	6.00	6.00	6.00
X_{Fe}	0.65	0.66	0.74	0.62	0.72	0.72	0.62	0.73	0.73	0.63	0.75

Sample	V2			V18		V5		
No. grain	5	3	4	1	1	1,2,3	8	8
Mineral	OpxI	OpxI	OpxI	OpxI	OpxI	OpxI	OpxI	OpxI
No. analyses	27	17	22	44	42	10 (Av)	31	34
Varieties	Pgt	Opx1H	Cpx1L	Cpx1L	Opx1H	Pgt	Opx1H	Cpx1L
n	1 (R)	1 (Lc)	1 (R)	1 (R)	1 (R)	14 (R)	1 (R)	1 (R)
SiO_2	48.71	47.38	49.43	49.67	48.34	47.06	46.49	49.23
TiO_2	–	0.10	0.13	–	0.14	0.03	0.08	–
Al_2O_3	–	–	0.23	0.54	0.14	0.16	–	0.20
Cr_2O_3	–	–	0.01	0.04	–	0.66	–	0.10
FeO*	37.19	41.97	20.63	21.61	43.07	41.36	47.09	24.26
MnO	0.89	1.10	0.53	0.05	0.49	0.54	0.69	0.25
MgO	8.18	9.00	7.33	6.39	7.26	5.56	4.85	4.57
CaO	5.37	0.64	21.14	21.39	0.69	4.82	0.92	20.97
Na_2O	0.08	–	0.36	0.13	–	0.14	–	0.29
K_2O	–	0.07	–	–	–	0.03	–	–
Total	100.42	100.26	99.79	99.82	100.13	100.36	100.12	99.87
Si	1.98	1.96	1.96	1.97	2.0	1.96	1.97	1.98
Al^{IV}	–	–	0.01	0.03	–	0.01	–	0.01
Ti	–	–	0.01	–	–	–	–	–
Cr	–	–	–	–	–	0.02	–	0.01
Fe^{2+}	1.27	1.45	0.69	0.72	1.49	1.44	1.67	0.82
Mn	0.03	0.04	0.02	–	0.02	0.02	0.03	0.01
Mg	0.5	0.56	0.43	0.38	0.45	0.35	0.31	0.28
Ca	0.23	0.03	0.9	0.91	0.03	0.22	0.04	0.91
Na	0.01	–	0.03	0.01	–	0.01	–	0.02
K	–	–	–	–	–	–	–	–
T Site	1.98	1.96	1.97	2.0	2	1.97	1.97	1.99
O Site	2.04	2.08	2.07	2.02	1.99	2.06	2.05	2.03
All	4.02	4.04	4.04	4.02	3.99	4.03	4.02	4.02
O	6	6	6	6	6	6	6	6
X_{Fe}	0.72	0.72	0.61	0.66	0.77	0.81	0.85	0.75

*Notes: n, numbers of analyses averaged; R, raster-scanning analysis; Lc, local (spot) analyses.
All iron as FeO. X_{Fe} = Fe/(Fe + Mg). All analytical results are available upon request to the corresponding author (V.I.F.).

(GSI) (Fonarev *et al.*, 1998). These inclusions correspond to a population of up to 15–20 inclusions in a given host mineral grain which, from criteria commonly used for ascertaining a relative inclusion chronology (e.g. Touret, 1981), have been trapped at the same time.

SAMPLE DESCRIPTION

As the Archaean high-grade basement rocks of the region are concealed everywhere beneath a sedimentary cover, core samples of exploratory drill holes have been used for this study. Representative samples of magnetite quartzites were collected from two localities – holes 3504 and 3588 (Fig. 1d). These rocks are of a dark grey colour and are medium- to coarse-grained, massive or more often banded (lenticular) because of alternating layers (from a few millimetres to 3–4 cm) of predominantly quartz or pyroxene–magnetite composition. The rocks have a granoblastic texture, sometimes with pyroxene porphyroblasts. The main assemblage consists of Opx (abbreviations after Kretz, 1983) and Cpx (both 20–25%) with quartz (35–50%) and magnetite (20–40%). Secondary grunerite is often present in these rocks in different quantities (1–3% in samples V16, V17 & V2 up to ~15% in samples V5 & V18). Garnet-bearing rocks Opx + Grt + Qtz + Mag (often with the secondary biotite) are less abundant. The chemical composition of magnetite quartzite from drill hole 3504 (depth 141.4 m) is (in wt%): $SiO_2 = 38.9$, $TiO_2 = 1.02$, $Al_2O_3 = 0$, $Fe_2O_3 = 14.06$, $FeO = 32.99$, $MnO = 0.03$, $CaO = 4.04$, $MgO = 5.47$, $Na_2O = 0.35$, $K_2O = 0.05$, $P_2O_5 = 0.27$, $SO_3 = 2.03$, total = 99.21 (Analytical Laboratory of Voronezh State University).

Both orthopyroxene and clinopyroxene occur as two generations (Fig. 2). The earliest generation, OpxI and CpxI, occurs in the form of subhedral crystals (porphyroblasts), which are often fractured and frag- mented and have uneven corroded boundaries. The grain size varies in different samples from ~50–200 μm (samples V5, V18) up to 0.5–1.5 mm (samples V16, V17). Orthopyroxene is often colourless and pleochroic from pinkish to pale brownish or yellowish shades. Clinopyroxene grains have a pronounced, often curved cleavage, a pale greenish colour and weak pleochroism. This generation of ortho- and clinopyroxene contains exsolution textures. The second generation of pyroxene (OpxII and CpxII) develops between grains of OpxI, and CpxI and in some cases in the large cracks in them (Fig. 2). These are small (about 20 μm) anhedral crys- tals which are often associated with acicular or prismatic grunerite (up to 0.5 mm). This grunerite develops after early generations of ortho- and clinopyroxene, which are preserved here only as small (50–100 μm) relics.

EXSOLUTION TEXTURES

The primary clino- and orthopyroxene (CpxP and OpxP) with the most widespread and diverse exsolu- tion textures in the magnetite quartzites studied are present in samples V16 (3504/153.5), V17 (3504/158), V18 (3504/162.5), V2 (3504/250), and V5 (3558/221.5). (Numbers correspond to drill hole number/depth.) Two types of exsolution textures are recognized in CpxI (Figs 3a,d,e,f,h,i & 4a,d,e). The first type of exsolution comprises relatively large (up to 5–10 μm) (0 0 1) lamellae (L) of orthopyroxene (Opx1L) in a host (H) matrix clinopyroxene (Cpx1H). The second exsolution type develops as very thin (~1 μm), relat- ively short and closely spaced (1 0 0) orthopyroxene
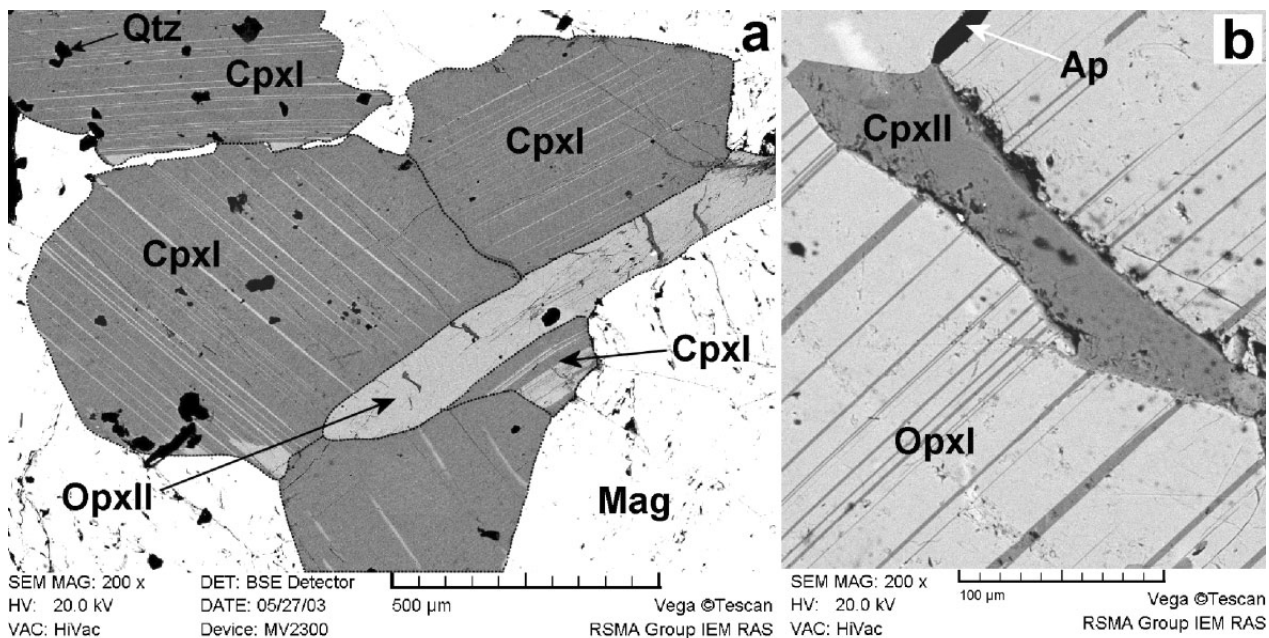

Fig. 2. BSE images of relationships between different generations of ortho- and clinopyroxene. Later generations OpxII (a) and CpxII (b) are developed in the interstices of the grains and the large cracks of the earlier generations (OpxI and CpxI). (a) Grain boundaries are shown by dotted line.
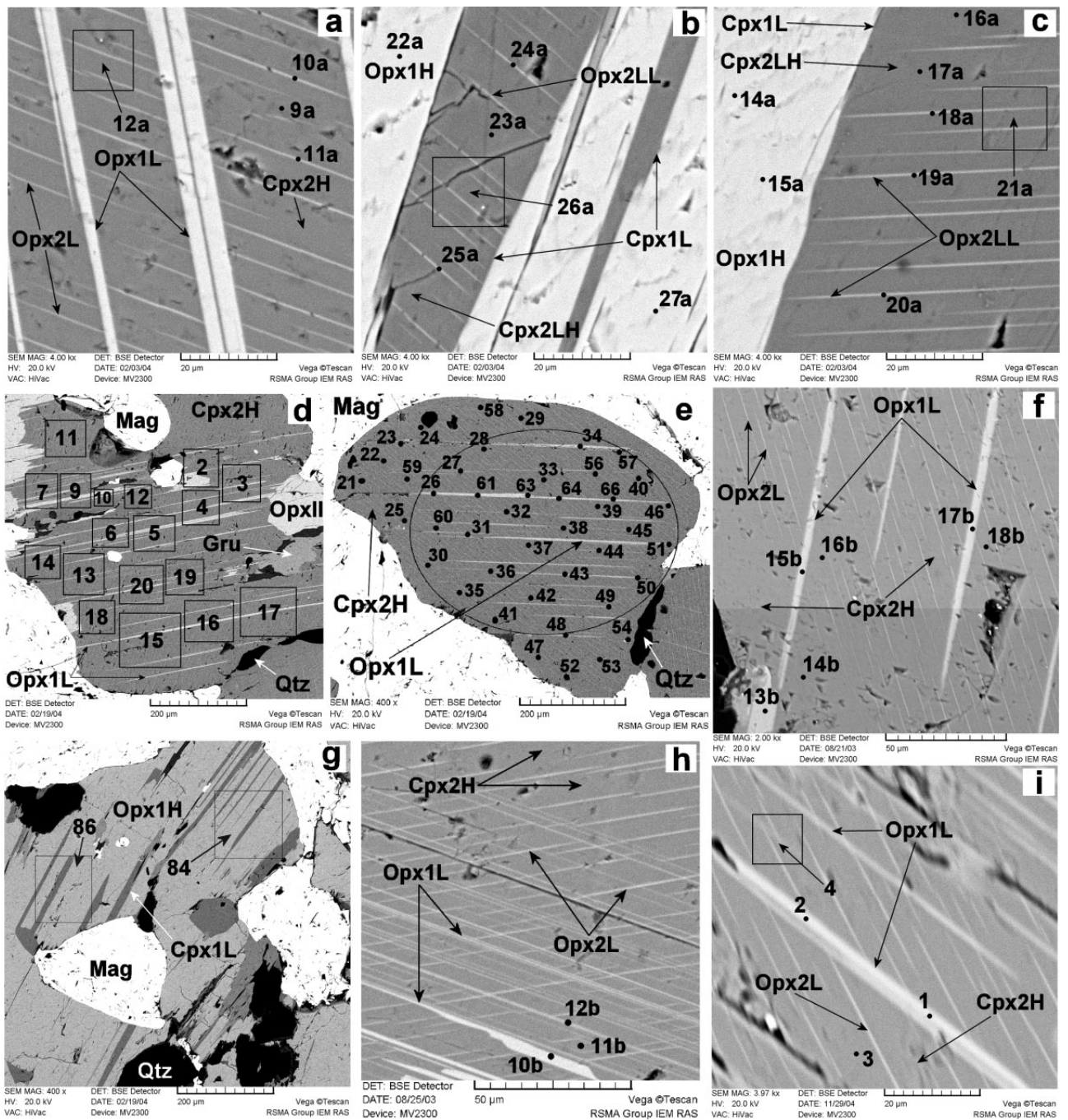
Fig. 3. BSE image of exsolution textures in pyroxene of high-grade BIF of VCM (samples V16 & V17). (a–h) Sample V16. (a) Clinopyroxene with large Opx1L lamellae (first-stage exsolution) and smaller Opx2L lamellae (second-stage exsolution). In all images the dark circles indicate the localities of microprobe analyses, and rectangles indicate raster-beam analyses. Numerals correspond to the numbers of analyses. (b), (c) Orthopyroxene with large clinopyroxene Cpx1L lamellae (first-stage exsolution), which in turn exsolved into Cpx2LH and Opx2LL. (d) Reintegration of the primary composition of clinopyroxene (raster-beam analysis). (e) Reintegration of the primary composition of clinopyroxene (compositional mapping by means of spot analyses). The contour shows the grain core used for reintegration (see text). (f) Evaluation of the composition of the second-stage exsolution products (Cpx2H) of primary clinopyroxene (spots 14b, 16b, 18b). (g) Reintegration of the composition of pigeonite (raster-beam analysis). (h) Evaluation of the composition of the early generation (Opx1L) of lamellae, which are exsolution products of primary clinopyroxene (spot 10b). (i) Sample V17. Exsolution textures of clinopyroxene with (0 0 1) Opx1L lamellae (first-stage) and (1 0 0) Opx2L lamellae (second-stage).
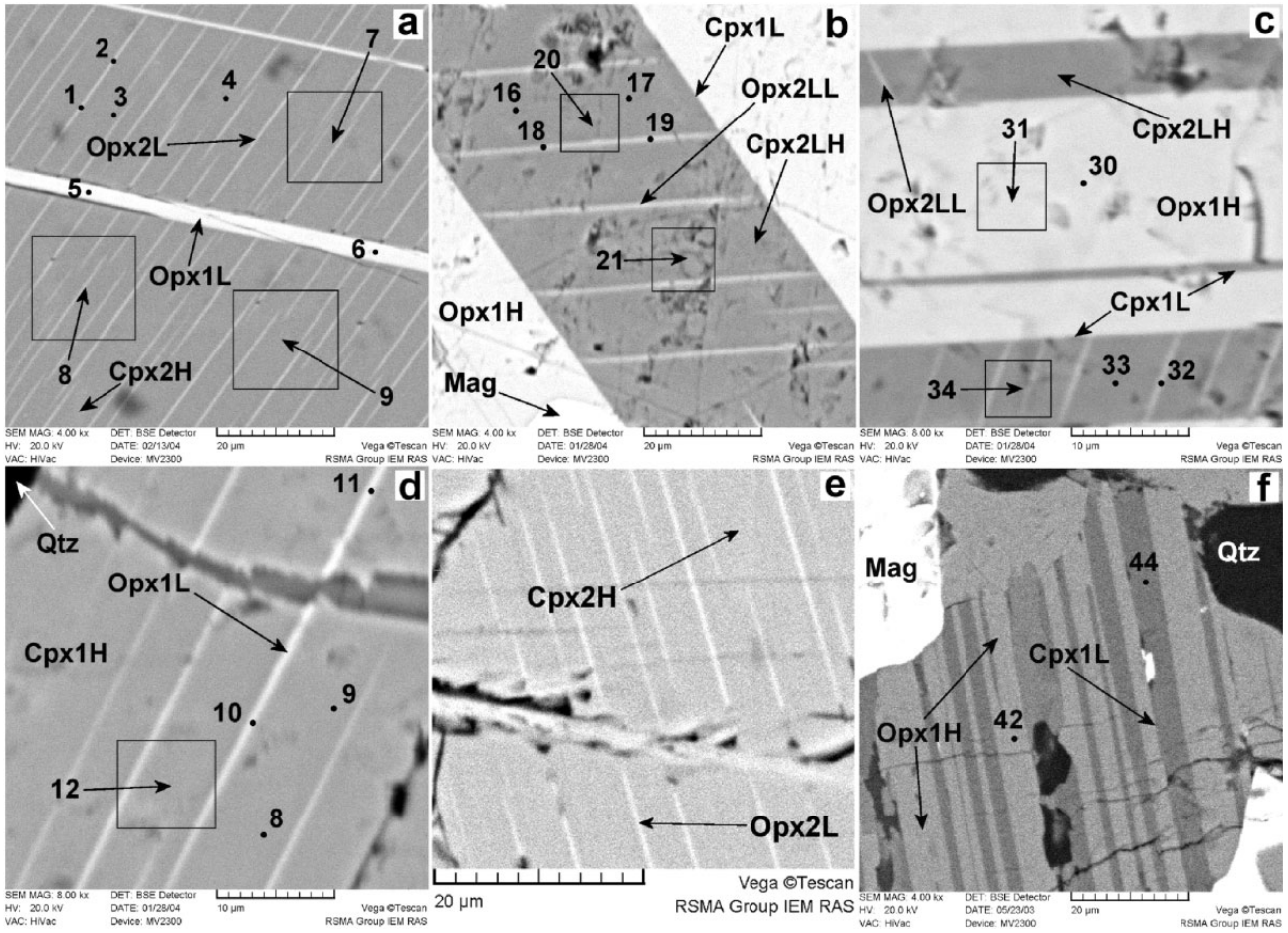
Fig. 4. BSE image of exsolution textures in pyroxene of high-grade BIF of VCM (samples V2, V5, V18). (a) Sample V2. Clinopyroxene with large orthopyroxene Opx1L lamellae and thinner Opx2L lamellae. (b)–(d) sample V5; (b, c) orthopyroxene with coarse clinopyroxene Cpx1L lamellae, which in turn break down into Cpx2LH and Opx2LL lamellae; (d) exsolution textures in clinopyroxene. (e, f) Sample V18. (e) Second-stage of clinopyroxene exsolution with Opx2L lamellae; (f) first-stage of orthopyroxene exsolution with Cpx1L lamellae.

lamellae (Opx2L) in the host clinopyroxene (Cpx2H). In some cases (samples V5, V18), no exsolution products from Cpx1H exsolution were detected, perhaps because of their very small sizes or absence in the plane of the thin sections. Orthopyroxene (Opx1) also displays two types of exsolution textures (Figs 3b,c,g & 4b,c,f). The first type is of coarse (up to 30–50 μm)

(0 0 1) clinopyroxene (Cpx1L) lamellae in the host orthopyroxene (Opx1H). In turn, clinopyroxene Cpx1L also breaks down with the exsolution of very thin ($< 1\ \mu m$) (1 0 0) numerous orthopyroxene (Opx2LL) lamellae in the host clinopyroxene (Cpx2LH).

A scheme of exsolution from primary clinopyroxene and orthopyroxene is shown in Fig. 5. The first
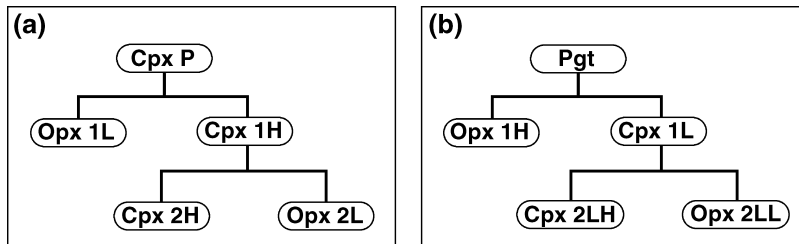
Fig. 5. Exsolution scheme of (a) primary clinopyroxene and (b) pigeonite in high-grade BIF of VCM. CpxP and Pgt are primary high-Ca and low-Ca (pigeonite) monoclinic pyroxenes, respectively; Opx1L and Cpx1H are the products of the first-stage exsolution of clinopyroxene; Opx1H and Cpx1L are the products of the first-stage exsolution of pigeonite; Cpx2H and Opx2L are the products of the exsolution of Cpx1H; Cpx2LH and Opx2LL are the exsolution products of Cpx1L.

generation of clinopyroxene (CpxI) corresponds morphologically to the primary clinopyroxene (CpxP) in this scheme. As will be demonstrated below, by analogy with earlier finds (Bonnichsen, 1969; Vaniman *et al.*, 1980; Sandiford & Powell, 1986; Harley, 1987) and consistent with its integrated composition, OpxI corresponds to the low-Ca clinopyroxene (pigeonite, Pgt).

Thus, the following equilibrium assemblages of pyroxenes can be distinguished in the samples studied (Fig. 5).

1 CpxP and pigeonite (in assemblage with magnetite and quartz) are the primary minerals. The Cpx chemistry is derived from the integrated composition of Opx1L + Cpx1H, while the pigeonite composition is derived from the integrated composition of Opx1H + Cpx1L.

2a Cpx1H and Opx1L are the exsolution products from the primary clinopyroxene (CpxP). The Cpx1H composition corresponds to the integrated composition of Cpx2H + Opx2L.

2b Opx1H and Cpx1L are the exsolution products of the primary pigeonite. The Cpx1L composition is derived from the integrated composition of Cpx2LH + Opx2LL.

3a Cpx2H and Opx2L are the exsolution products of Cpx1H.

3b Cpx2LH and Opx2LL are the exsolution products of Cpx1L. In addition, textural relationships indicate that the second generations of ortho- and clinopyroxene are also equilibrated (in the presence of magnetite, quartz and grunerite).

4 OpxII + CpxII + Gru + Mag + Qtz.

Finally, an equilibrium distribution of components may be anticipated at contacts between the mineral grains of CpxI(rim) + OpxI(rim), CpxII(rim) + OpxII(rim), etc. None of these mineral assemblages, which characterize retrograde processes, is discussed in this paper.

MINERAL CHEMISTRY

As mentioned above, the reintegration of the primary pyroxene compositions poses a problem when, in most cases, not all exsolution products are present at the surface of the thin section. For this reason, several mineral grains and even samples were rejected after microscopic and microprobe examination. The best exsolution textures are developed in samples V16, V2, V5 and V18 for which the fullest results were obtained.

The *primary clinopyroxene* (CpxP) composition was obtained for different grains in sample V16 by raster scanning and compositional mapping with spot analyses. Scanning over fields of 40–80 μm (18 raster fields within a grain) covered virtually the whole area of the grain approximately 400×500 μm (Fig. 3d). The iron mole fraction (X_{Fe}) of the mineral varied from 0.64 to 0.66 (Table 1), and the average Ca concentration was 17.26 ± 1.3 wt% (Fig. 6a).

Analysis by means of compositional mapping (about 60 spot analyses) was restricted to the core of the grain (about 0.2 mm), because, as seen in Fig. 3(e), the periphery contains no orthopyroxene lamellae of the first exsolution stage (Opx1L). Obviously, this can be caused by the later (before the exsolution of the second array of Opx2L lamellae) redistribution of components between the coexisting minerals. The CaO content in the primary clinopyroxene determined by this method is 14.86 wt% at a Fe mole fraction of 0.66 (Table 1, Fig. 6a).

The reintegrated composition of the *primary pigeonite* was estimated in raster mode (see, e.g. Fig. 3g, fields 84, 86) for samples V16 and V2. In the three grains from sample V16 that were analysed, the CaO concentrations of the mineral are 3.05, 4.45 and 6.23 wt% with Fe mole fraction of 0.73, 0.72 and 0.72 respectively (Fig. 6b). Similar compositions are found for sample V2 (five raster fields 100–200 μm each) with 3.82–5.35 wt% CaO and iron mole fractions in the 0.71–0.72 range (Fig. 6d, Table 1). Obviously, these analyses will have, as demonstrated above, underestimated CaO contents, but even the lowest of these values is atypical of orthopyroxene and suggests that it was produced by the exsolution of primary pigeonite with transition from the monoclinic to orthorhombic structures, as determined in analogous situations (Bonnichsen, 1969; Vaniman *et al.*, 1980; Sandiford & Powell, 1986; Harley, 1987).

The compositions of the first-stage *exsolution products of the primary clinopyroxene* (Cpx1H & Opx1L) were determined in samples V16 & V2. The composition of Cpx1H (integrated Cpx2H & Opx2L) was obtained by analysing, in raster mode (10–20 μm), samples V16 and V2 that had a high proportion of Opx2L lamellae (Fig. 3a, field 12a; Fig. 4a, fields 7,8,9; Fig. 6a,c; Table 1) and, hence, a good analytical precision (CaO = 20.52 ± 0.7 wt%, iron mole fraction is 0.61 ± 0.13). The CaO content and iron mole fraction of the Opx1L exsolution lamellae (e.g. Fig. 3h, point 10b; Fig. 4a, points 5,6) are 0.79 ± 0.09 wt% and 0.75 ± 0.001 respectively.

A slightly higher CaO content (21.23 ± 0.3 wt%) in samples V16 and V2 and, correspondingly, a lower iron mole fraction (0.6 ± 0.005) were determined for Cpx2H produced during the second-stage exsolution (Fig. 5) of the CpxP (Fig. 3a, point 9a; Fig. 3f, points 14b, 16b, 18b; Fig. 4a, points 3, 4 and others; Fig. 6a,c). Such increase in the CaO content in products (Cpx1H, Cpx2H) of different exsolution stages of the primary clinopyroxene (CpxP) is compatible with the stability of the clino–orthopyroxene assemblage at decreasing temperature (Lindsley, 1983). It was not possible to determine the composition of the orthopyroxene lamellae (Opx2L) produced by the exsolution of Cpx1H. This was because of the small sizes of these lamellae, their analyses usually contained excess CaO and MgO due to the overlapping of the host mineral.
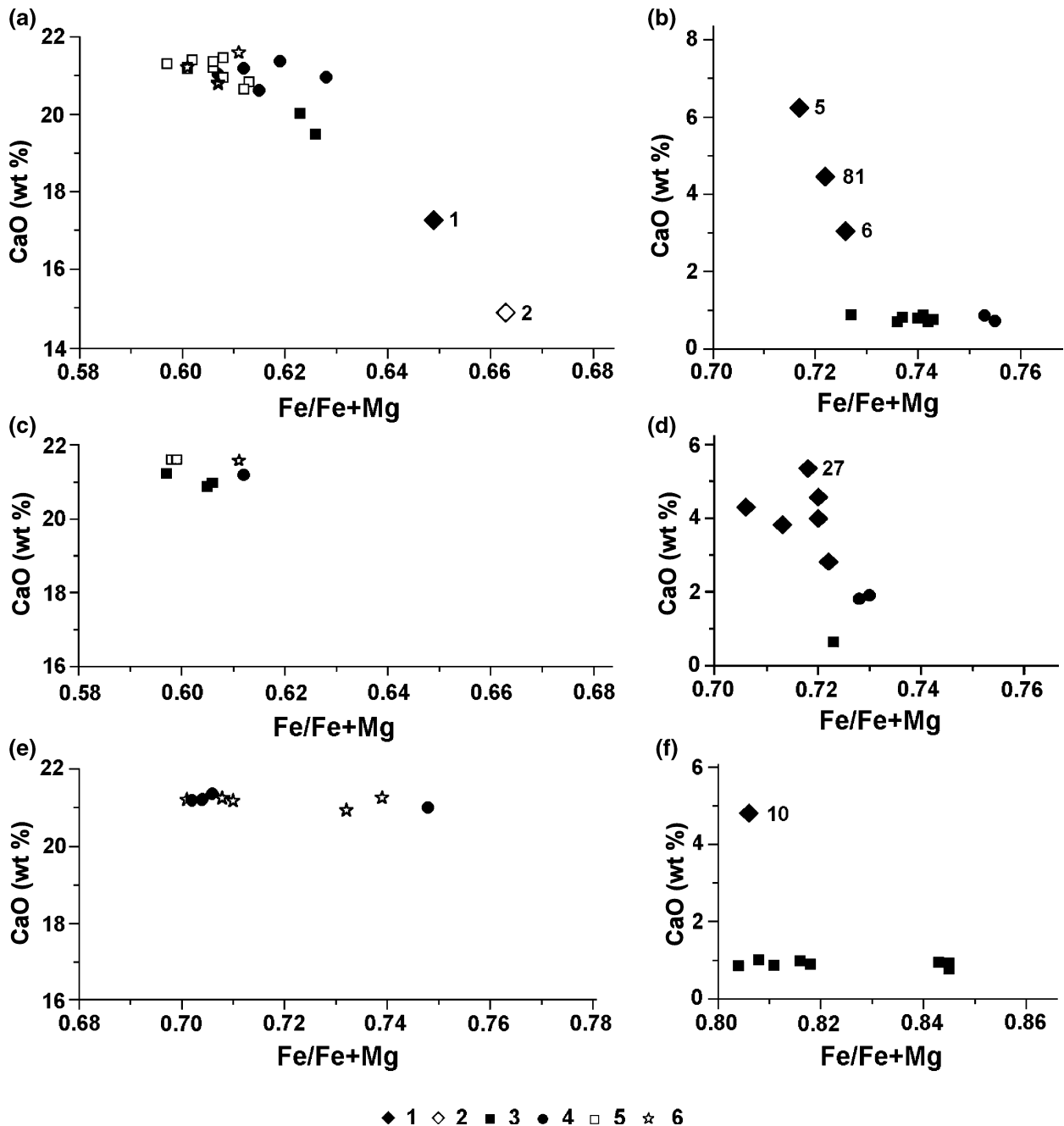
Fig. 6. Pyroxene composition in high-grade BIF of VCM: sample V16 (a – Cpx, b – Opx and Pgt); sample V2 (c – Cpx, d – Opx and Pgt); sample V5 (e – Cpx, f – Opx and Pgt); 1 – CpxP and Pgt (raster-scanning), 2 – CpxP (compositional mapping with spot analyses); 3 – Cpx1H, Opx1H; 4 – Cpx1L, Opx1L; 5 – Cpx2H; 6 – Cpx2LH. Numerals in the diagram correspond to the numbers of microprobe analyses of the primary (integrated) clinopyroxene and pigeonite.

The composition of the first-stage *exsolution products of the primary pigeonite* (Opx1H & Cpx1L) was determined in samples V16, V2 and V18. The CaO concentration and iron mole fraction of the early orthopyroxene (Opx1H) in samples V16 and V2 (Fig. 3b,c, points 22a, 27a, 14a, 15a) are 0.77 ± 0.08 wt% (on average) and 0.74 ± 0.01 respectively. Somewhat higher iron content (0.77) is

found for the Opx1H lamellae from sample V18 (Table 1), probably, because of the local differences of the bulk chemistry of the rock. Clinopyroxene lamellae in the orthopyroxene from samples V16 and V2 yielded similar compositions: Cpx1L and Cpx2LH (CaO = 21.05 ± 0.26 wt%, X_{Fe} = 0.62 ± 0.01 and CaO = 21.11 ± 0.38 wt%, X_{Fe} = 0.61 ± 0.004 respectively; Table 1).
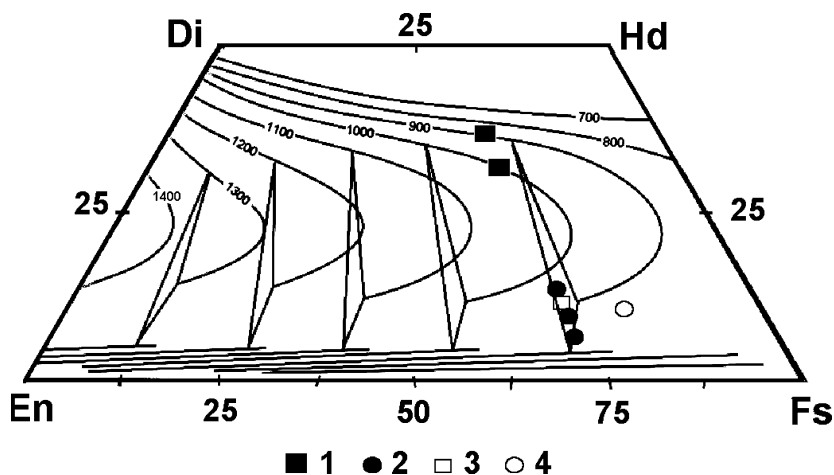
Fig. 7. Polythermal diagram of the compositions of coexisting Cpx, Opx, and Pgt for $P = 10$ kbar (Lindsley, 1983). 1, 2 – Compositions of primary Cpx and Pgt in sample V16; 3, 4 – compositions of primary Pgt in samples V2 (3) and V5 (4).

Somewhat higher CaO contents (21.43 wt%) and iron mole fraction ($X_{Fe} = 0.66$) are found for Cpx1L lamellae from sample V18 (Table 1) as well. Figures 3(b,c) and 4(f) show examples of BSE images with lamellae Cpx1L (fields 21a & 26a, point 44) and Cpx2LH (points 16a, 17a & 23a). As with the clinopyroxene, it was not possible to determine the composition of the orthopyroxene lamellae (Opx2LL) of the second exsolution stage of the primary orthopyroxene (exsolution of Cpx1L).

Sample V5 has the highest Fe mole fractions of all minerals (Fig. 6e,f; Table 1) because of the more ferrous bulk chemistry of the rock. Here, the composition of the primary pigeonite was estimated by raster-beam microprobe analysis (14 fields 100–200 μm in size) of different grains of the first orthopyroxene generation (OpxI) that had clearly pronounced exsolution textures (Fig. 4b,c). The average CaO and iron mole fraction of this primary pigeonite are 4.8 wt% and 0.81 respectively (Table 1). As in the previous samples, this CaO concentration may be slightly underestimated (and, correspondingly, the iron mole fraction is an overestimate). In addition, the average compositions of exsolution products of this primary pigeonite are Opx1H (CaO = 0.92 ± 0.06 wt%, $X_{Fe} = 0.82 \pm 0.02$), Cpx1L (CaO = 20.4 ± 1.75 wt%, $X_{Fe} = 0.72 \pm 0.02$) and Cpx2LH (CaO = 21.14 ± 0.14 wt%, $X_{Fe} = 0.71 \pm 0.01$). Because of the small sizes of the exsolution products of the primary clinopyroxene in this sample (Fig. 4d), it was not possible to estimate their compositions.

THERMOMETRY

Temperatures of the primary pyroxene formation have been established using the experimental data of Lindsley (1983) at a pressure of 10 kbar. Primary clinopyroxene (CpxP) with CaO concentrations of 17.26 and 14.86 wt% (Sample V16) in association with pigeonite in sample V16 is estimated to be stable at temperatures of > 900 °C and 1000 °C with allowance for the probable (undetected) CaO overestimation for CpxP (Fig. 7). The effect of pressure on the stability of this association is insignificant (Lindsley, 1983), which practically eliminates the necessity of pressure corrections over the range 5–15 kbar. At temperatures of > 900 °C, the stable phase is also the most calcic pigeonite (CaO = 5.35–6.23 wt%) with a Fe mole fraction of 0.717and 0.718 (samples V16 & V2 respectively). According to the temperature dependence of the Fe mole fraction (Lindsley, 1983), pigeonite with such a Fe/Mg ratio should be stable at a temperature of 920 °C in the assemblage with ortho- and clinopyroxene (Fig. 8) and at higher temperatures in assemblages with clinopyroxene alone (Figs 7 & 8). Similar limiting crystallization temperatures (> 900 °C) were also obtained for other pigeonite grains with lower estimated CaO contents and higher Fe mole fraction (Table 2).

The temperatures of the first stage of the primary clinopyroxene (CpxP) and pigeonite exsolution to form the assemblages 2a (Cpx1H + Opx1L) and 2b (Opx1H + Cpx1L), respectively, were calculated using the two-pyroxene (ortho–clinopyroxene) thermometer (Fonarev & Graphchikov, 1991). This thermometer is based on experimental results first obtained (Fonarev & Graphchikov, 1982) at rather low temperatures (750–800 °C) and according to the critical evaluation of Fonarev & Graphchikov (1991), it yields the most accurate results over the temperature range 900–1000 °C when compared with all other versions. Unfortunately, the thermometer of Lindsley (1983) is inconvenient for correct estimations of pyroxene stability at relatively low temperatures because of the graphic presentation. Moreover, according to Lindsley (1983), because of discrepancy 'a number of the dissolving experiments at 810 ± °C' the thermometer is more reliable at higher temperatures. In turn, the two-pyroxene (ortho–clinopyroxene) thermometer of Fonarev & Graphchikov (1991) could not be used for the clinopyroxene–pigeonite assemblage (at high temperatures). Very similar temperatures of 705 °C and
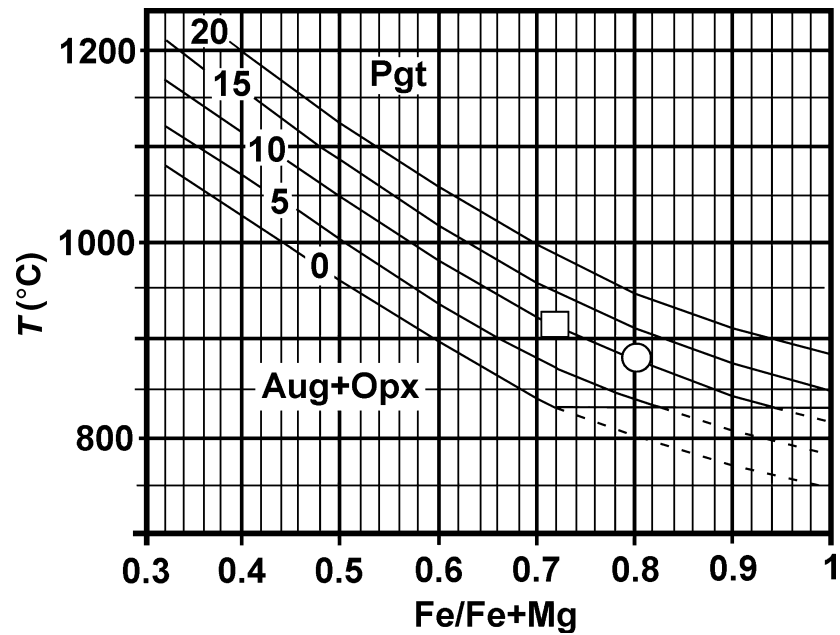
Fig. 8. Minimum stability temperature of pigeonite *v.* clinopyroxene + orthopyroxene as a function of the Fe mole fraction of the mineral (Lindsley, 1983). Curves correspond to pressures 0–20 in kbar. The square corresponds to the compositions of pigeonite in samples V16 and V2, the circle corresponds to pigeonite compositions in sample V5.

Table 2. Temperatures crystallization and exsolution of pyroxenes from BIF of the Voronezh Crystalline Massif.

Sample	Mineral (gener.)	Varieties	n	No. analyses	X_{Fe}	CaO, wt%	2Px	Lind (1)	Lind (2)
V16	Cpx1	CpxP	16 (R)	1 av (2–10,13–20)	0.65	17.26		>900	
	Cpx1	CpxP	32 (Lc)	2 av (26–28,31–46,48–50,54–56,57,60,61,63,64,66)	0.66	14.86			1000
	Cpx1	Opx1L	2 (Lc)	3 av (10b,13b)	0.75	0.79	705		
		Cpx1H	2 (R)	4 av (6a,12a)	0.63	19.66			
	Opx1	Pgt	1 (R)	81	0.72	4.45		>900	
	Opx1	Pgt	2 (R)	5 av (84,86)	0.72	6.23		>920	
	Opx1	Pgt	2 (R)	6 av (28a,29a)	0.73	3.05		>900	
	Opx1	Opx1H	4 (Lc)	7 av (69,73,75,80)	0.74	0.73	694		
		Cpx1L	3 (Lc)	8 av (71,74,79)	0.62	21.12			
	Opx1	Opx1H	2 (Lc)	9 av (22a,27a)	0.73	0.84	709		
		Cpx1L	1 (R)	26a	0.62	20.61			
V2	Opx1	Pgt	1 (R)	27	0.72	5.35		>920	
	Opx1	Opx1H	1 (Lc)	17	0.72	0.64	708		
		Cpx1L	1 (R)	22	0.61	21.19			
V18	Opx1	Opx1H	1 (R)	42	0.77	0.69	688		
		Cpx1L	1 (R)	44	0.66	21.43			
V5	Opx1	Pgt	13 (R)	10 av (6–18)	0.81	4.80		>880	
	Opx1	Opx1H	1 (R)	31	0.85	0.92	679		
		Cpx1L	1 (R)	34	0.75	21			

*2Px – two pyroxene thermometer (Fonarev & Graphchikov, 1991); Lind 1 – fig. 8 in Lindsley (1983); Lind 2 – fig. 9 in Lindsley (1983). For other notes see Fig. 1.

688–709 °C (Table 2) were determined for samples V16, V18 and V2 (Table 2) for assemblages 2a and 2b respectively (the exsolution of the primary clinopyroxene and pigeonite).

In sample V5, pigeonite with $X_{Fe} \leq 0.81$ (Table 1) should be stable in assemblage with clinopyroxene (Lindsley, 1983) at temperatures above 880 °C (Fig. 8). The Fe mole fraction of Opx1H varies from 0.8 to 0.84 at a relatively constant CaO concentration of about 0.85 wt% (Table 1). The exsolution products of the clinopyroxene do not exhibit any significant variations in the CaO contents (20.65–21.57 wt%); their Fe mole fraction unsystematically ranges over a interval of 0.7–0.75, perhaps, because of the insufficient accuracy of the raster-beam analysis of the integrated composition of most Cpx1L lamellae. An exception seems to be the Cpx1L at point 34 (Figs 4c & 6e), which was used, together with matrix Opx1H (point 31) in contact with it, to evaluate the temperature (680 °C) of the first exsolution stage of the primary orthopyroxene (Opx1). It was not possible to determine the temperature of the second exsolution stage of clinopyroxene in the samples studied because of the absence of accurate data on the chemistry of Opx2L and Opx2LL lamellae.
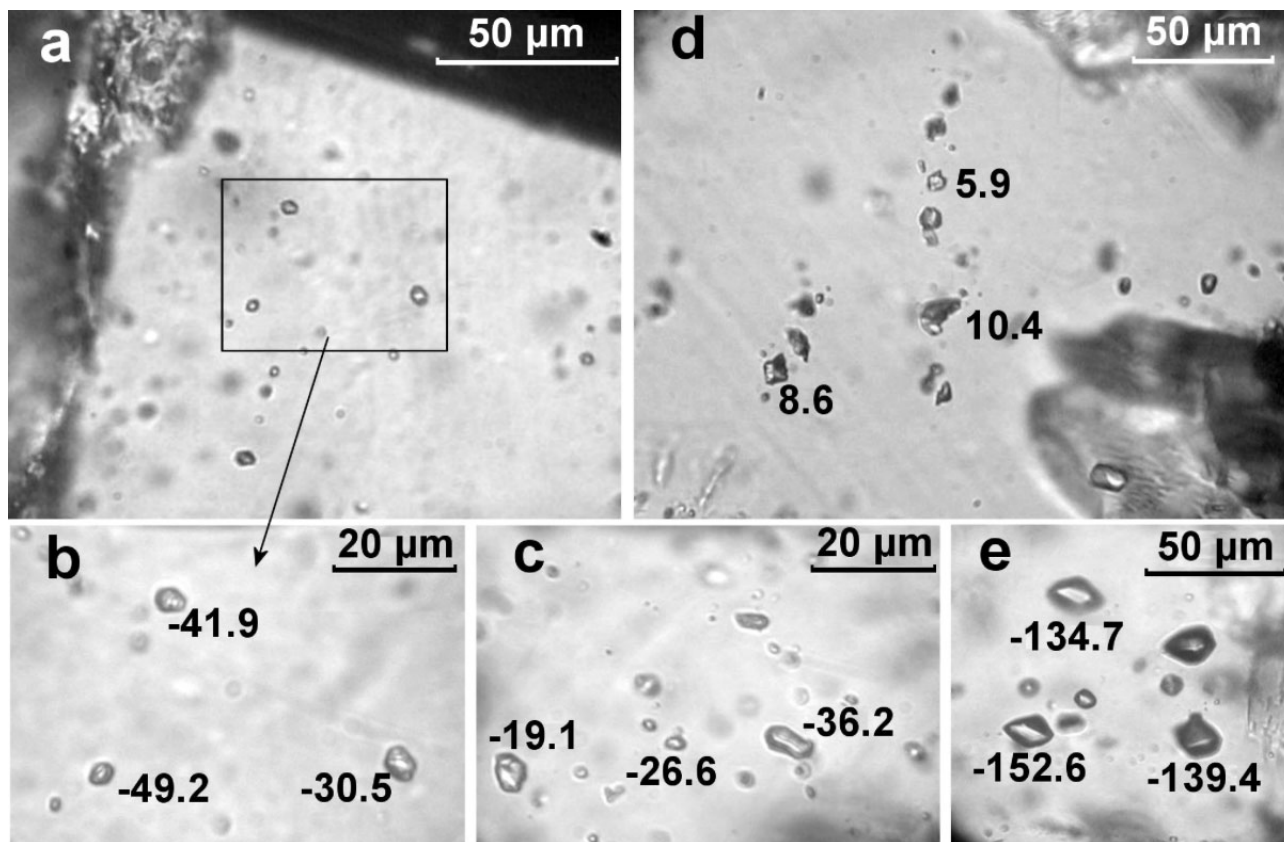
FLUID INCLUSIONS

A detailed description of the fluid inclusions from metamorphic rocks of the VCM region studied is beyond the scope of this paper. Here, only data which are necessary to evaluate the peak metamorphic conditions of the BIF in the region are presented. Moreover, only the samples studied containing pyroxene with exsolution textures will be examined (V2, V5, V16, V17 & V18). Inclusions in quartz from these samples are mostly CO_2-rich (with subordinate amounts of nitrogen), pure nitrogen, nitrogen-aqueous, and brine varieties.

The CO_2-rich inclusions are usually no greater than 5–20 μm (more rarely up to 50–70 μm), and some samples contain numerous smaller inclusions that were not suitable for accurate measurements. Inclusions are most often round or oval, sometimes subhedral and with negative crystal shape. The largest inclusions have an irregular shape as a result of post-trapping decrepitation. The inclusions are mostly concentrated in the form of isolated groups (primary inclusions, Fig. 9a–c), or spatially restricted to healed cracks (pseudosecondary inclusions, Fig. 9d), or, very rarely, are hosted by healed cracks that intersect grain boundaries (secondary inclusions). Two generations of CO_2-rich inclusions (Fig. 10) can be distinguished which differ by textural features (primary, pseudosecondary), location in various parts of the host grains (the central parts, periphery), shapes, and temperatures of homogenization (T_h), i.e. density (ρ).

First-generation (FLI) inclusions are represented by primary inclusions of high density ($\rho = 1.102$–1.152 g cm^{-3}) with very low T_h (to liquid): -36.7 to -49.2 °C (Fig. 10). Temperatures of homogenization of CO_2-rich inclusions and, correspondingly, their densities notably vary, with values reaching $\sim$13–15 °C (e.g. sample V17). In most cases these variations, which are common in metamorphic rocks, are the result of partial fluid leakage during post-trapping evolution.

The melting temperatures (T_m) of these inclusions vary from -56.9 to -57.9 °C. Such melting point depression in comparison with pure carbon dioxide (-56.6 °C) is caused by admixtures of additional components (nitrogen, methane, noble gases, etc.). High-density carbonic inclusions are best preserved in samples V16, V17 and V18 (Fig. 10), with the highest density inclusion found in sample V18. These

Fig. 9. Photomicrograph of fluid inclusions in high-grade BIF of VCM. (a)–(c) Primary CO_2-rich inclusions in different grains of quartz in sample V18 [(a) and (b) inclusions of highest-density at different magnifications]. (d) Pseudosecondary CO_2-rich inclusions in sample V2; (e) primary nitrogen (N_2–CH_4) inclusion in sample V16. Crossed polarizers.
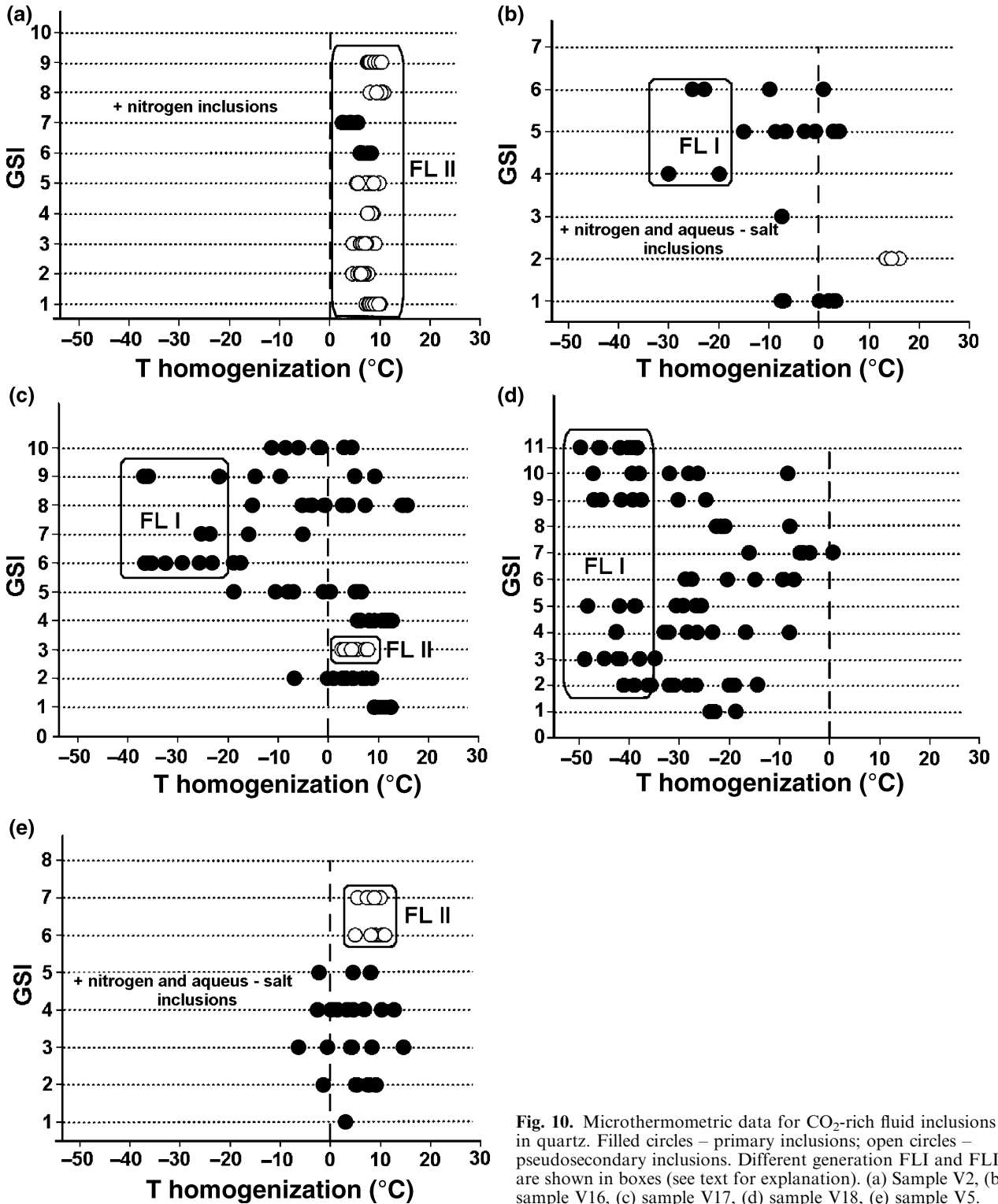
Fig. 10. Microthermometric data for CO_2-rich fluid inclusions in quartz. Filled circles – primary inclusions; open circles – pseudosecondary inclusions. Different generation FLI and FLII are shown in boxes (see text for explanation). (a) Sample V2, (b) sample V16, (c) sample V17, (d) sample V18, (e) sample V5.

inclusions are light, relatively small (no more than 5 μm) with sharp boundaries, round, with the largest of them showing the morphologies of negative crystals. They are grouped in the cores of quartz grains

(Fig. 9a,b) and were trapped at the time of its crystallization.

Second-generation (FLII) inclusions are represented by pseudosecondary CO_2-rich inclusions (Figs 9d &
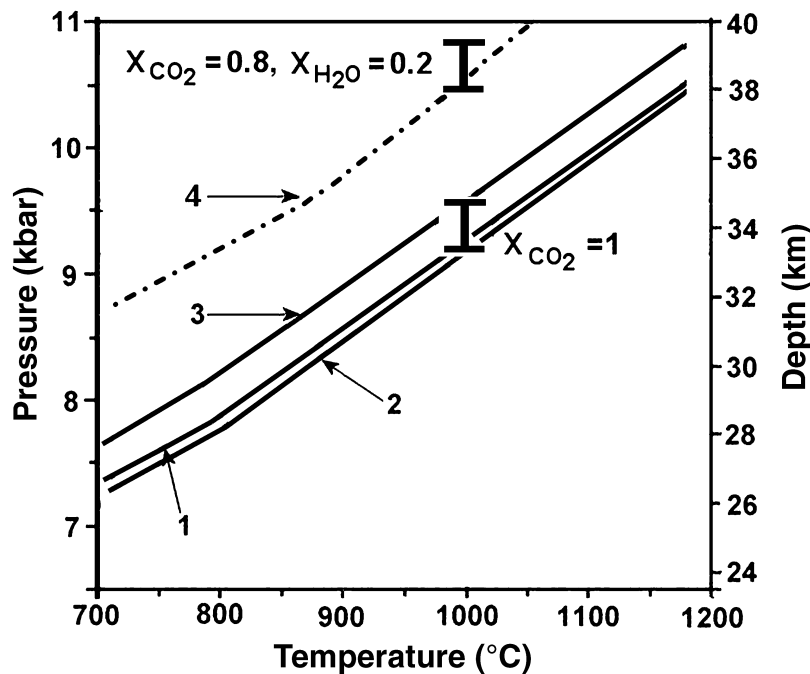
Fig. 11. *P–T*–depth conditions of the peak (primary) metamorphism of BIF of the Voronezh crystalline massif calculated for *T* = 1000 °C and X_{CO_2} = 1 and 0.8 (data of mineralogical thermometry and microthermometry of fluid inclusions, respectively, see text). Curves are isochores of the densest carbon dioxide inclusions with Th = −49.2 °C. 1–3 – Isochores for fluid with X_{CO_2} = 1 (ρ = 1.152 g cm^{-3}) after 1 – Belonoshko & Saxena (1991), 2 – Duan *et al.* (1992, 1996, 3 – Span & Wagner (1996); 4 – isochore for fluid with X_{CO_2} = 0.8, X_{H_2O} = 0.2 (ρ = 1.142 g cm^{-3}) after Duan *et al.* (1992, 1996. Bars show the pressure interval for different approximations of the *P–V–T* data.

10) with densities ranging from 0.899 to 0.854 g cm^{-3} (T_h from 4.6 to 10.9 °C). Their melting temperature varies from −56.9 to −58.1 °C. These are oval inclusions located along healed cracks usually in the periphery of quartz grains.

Nitrogen and nitrogen-aqueous inclusion with CH$_4$ ranging from 12 to 39 mol% (Raman analyses) were found in samples V2, V5 and V16. There are primary (Fig. 9e) or rarer pseudosecondary inclusions of irregular (30–70 μm), oval or negative crystal (20–30 μm) shape. They are clustered in the cores or periphery of quartz grains. In many cases, these inclusions are associated with primary CO$_2$-rich inclusions. Their temperatures of homogenization varies from −131 °C to −152.6 °C in samples V2 and V16 and they are higher (from −115.9 °C to −122.1 °C) in sample V5. Some N$_2$-rich inclusions contain a small quantity of water with a melting temperature from −0.2 to −0.4 °C.

Aqueous-salt inclusions were found in samples V5 and V16. These inclusions are typically light, isometric, with size is no more than 5–10 μm. In most cases, they occur along healed cracks as within separate grains (pseudosecondary) and crosscutting the grain boundaries (secondary). Final melting temperatures range from −1.1 to −3 °C.

BAROMETRY

The occurrence of high-density (ρ = 1.152 g cm^{-3}) carbon dioxide inclusions in minerals of the BIF, along with the calculated temperature of the primary pyroxene crystallization opens the unique possibility of estimating the peak metamorphic pressure. Figure 11

presents isochores of these densest CO$_2$-rich inclusions according to the latest approximations of the *P–V–T* data (Belonoshko & Saxena, 1991; Duan *et al.*, 1992, 1996; Span & Wagner, 1996). Their comparison with the temperature of the primary pyroxene crystallization (≥1000 °C) indicates that the rocks were originally metamorphosed not only at UHT but also under relatively high pressure ≥9.2–9.6 kbar. This pressure corresponds to the measured pure CO$_2$ inclusions which, as mentioned above, could lose part of the fluid (mostly water) during the post-trapping evolution. Thus, it is partial pressure of CO$_2$ (P_{CO_2}) which is usually lower than the total pressure (P_{tot}). For the majority of granulite complexes, the common P_{CO_2}/P_{tot} ratio is equal to 0.7–0.8 (X_{H_2O} = 0.2–0.3) (see for example, Harris & Jayaram, 1982; Fonarev *et al.*, 2003; Maaskant, 2004). Taking into account this X_{H_2O} value, the total metamorphic pressure of the BIF of the region was calculated as ≥10–11 kbar, i.e. the rocks were metamorphosed at depths of at least 36–40 km (Fig. 11).

DISCUSSION AND CONCLUSION

The unique pyroxenes with exsolution textures recently discovered in the BIF of the VCM permits the evaluation of the peak temperature of metamorphism of these rocks to be ≥1000 °C. This value is derived for the least calcic of the reintegrated primary clinopyroxene compositions (Fig. 7, Table 2) using pyroxene quadrilateral thermometry (Lindsley, 1983). This temperature value is corroborated by estimates obtained using the reintegrated pigeonite composition and its temperature of minimum stability (Lindsley,

1983) relative to Cpx and Opx as a function of iron content (> 900–920 °C for relative magnesian compositions from samples V16 and V2, > 880 °C for more ferrous pyroxene from sample V5). These values are similar to the 'very high temperatures' of > 980 °C obtained for the Archaean iron formations in the Napier Complex, Enderby Land, Antarctica (Harley, 1987).

The breakdown of the early low-calcic clinopyroxene (pigeonite) into Opx1H and Cpx1L (Fig. 5) in the magnetite quartzites of the VCM is determined to have taken place at 700 ± 15 °C (two-pyroxene thermometer of Fonarev & Graphchikov, 1991). The exsolution of the early clinopyroxene generation into Cpx1H and Opx1L is also estimated to have taken place at a similar temperature of 705 °C. This breakdown scheme differs from that developed in the Napier Complex where clinopyroxene exsolution into secondary pigeonite, with a slightly higher Fe mole fraction than in the primary mineral, reportedly occurred at 930–970 °C (Harley, 1987). Obviously, the exsolution temperature obtained for pigeonite (700 ± 15 °C) does not correspond to its stability limit of > 800 °C (Lindsley, 1983). There are good reasons to believe that exsolution took place metastably, or there are some intermediate pyroxene modifications whose traces were not found as of yet (or were not preserved).

Two generations of CO_2-rich fluid inclusions, different generations of the ortho-and clino-pyroxenes (I and II), presence of the secondary grunerite, etc. indicate multistage metamorphism with regressive post-peak events. The peak conditions ($T = 1000$ °C) were characterized by the CO_2-dominated high-density fluid with some fraction of the N_2-rich ($\pm$ methane) gas (according to the primary character of the corresponding fluid inclusions). The characteristics of fluid inclusions allowed the pressure and depth of the metamorphism to be estimated as 10–11 kbar and 36–40 km respectively.

Exsolution textures in pyroxenes in BIF are not commonly reported, although there are three reports from the Biwabik Iron Formation in Minnesota (Bonnichsen, 1969), the Stillwater Iron Formation in Montana (Vaniman *et al.*, 1980) and the Napier Complex, Enderby Land (Sandiford & Powell, 1986; Harley, 1987). But the first two localities are the result of contact metamorphism and in general, they do not characterize Precambrian geodynamic conditions. The high temperatures and pressures of the regional metamorphism found for the VCM are not known for other Precambrian BIF areas, apart from the Archaean meta-ironstone of the Napier Complex (Sandiford & Powell, 1986; Harley, 1987). Temperatures of metamorphism of most high-grade Precambrian BIF were estimated in the range of 650–750 °C at a pressure of 3–8 kbar (e.g. Gole & Klein, 1981; Mahabaleswar, 1986; Fonarev, 1987; Zhai & Windley, 1990) with the rare exception of 770–850 °C and 9–11 kbar (Krogh, 1977; Devaraju & Laajoki, 1986; Savko, 1999a). A

peak metamorphic temperature of 980–1020 °C was found for the meta-ironstone of the Napier Complex. Pressure was not estimated for these rocks specifically; however, values similar to those determined here for the VCM (10–11 kbar) were obtained for garnet–orthopyroxene-bearing granulites of the Napier Complex in the Scott Mountains and Khmara Bay region (Harley, 1985). The UHT metamorphism for the Napier complex was attributed to the emplacement and migration of magmas and controlled by water-undersaturated or dry melting reactions (Harley, 1987) near the base of the continental crust (Sandiford & Powell, 1986). It is envisaged that a similar process could have given rise to the UHT conditions of VCM also.

As mentioned earlier, the high-grade magnetite quartzites of the region are closely associated with the Archaean metaultrabasites and metagabbroids metamorphosed at granulite facies conditions (Savko, 1999b). Metaultrabasites are conformable with the host rocks and form layers and lense-like bodies with lengths of 150–200 m to 7500 m, and thicknesses from 50 to 100 m. They are slightly differentiated and correspond to peridotite–pyroxenite ultramafic rock types. Metagabbroid rocks show crosscutting relationships with the metaultrabasites. This variety of rocks indicates the existence of a deep heat source originating in the asthenosphere or mantle. Together with the heat flow from this source, the metaultrabasites and metagabbroids would have provided the necessary temperature for metamorphism of the BIF reported here. These peak conditions were characterized by the CO_2-dominated high-density fluid with some fraction of the N_2–CH_4-rich gas (according to the primary character of the corresponding fluid inclusions).

The new data on the high-temperature peak metamorphism of the BIF of the VCM represented here, testify to multistage metamorphic and tectono-thermal history of the region. The few previous P–T estimates do not exceed 700–850 °C, at pressures of $\sim$5–7 kbar (Savko, 1999a). These estimates were obtained using the compositions of exsolved primary and late (newly formed) pyroxenes. With reference to the pattern of pyroxene development reported here, the results from Savko (1999a) correspond to the retrograde (post-peak) metamorphic stage. As mentioned above, multistage metamorphism is confirmed by the presence of various generations of ortho- and clinopyroxenes (I and II), secondary grunerite in the investigated rocks, as well as at least two generations of CO_2-rich fluid inclusions. Unfortunately, at present there are no data that allow the P–T path of metamorphism of the region to be made more specific. The interpretation of Shchipansky & Bogdanova (1996) is that the Oskol Domain of VCM and the Azov Block of the Ukrainian Shield can be considered as a single Oskol-Azov Domain (Fig. 1b). High-grade BIF of these regions have closely similar textures, mineralogy and mineral compositions. Detailed investigations of T–P–f_{O_2} metamorphic con-

ditions were carried out for the Mariupole ore field of the Azov Block (Fonarev, 1987). The obtained results (695 ± 20 °C, 5 kbar) correspond to the data of Savko (1999a) for the VCM and also characterize one of the retrograde metamorphic events. Absolute age data for the Azov Block (Shcherbak *et al.*, 1984, 1993) have identified three tectono-thermal (metamorphic) events with the ages of 3.45, 2.9–2.8 and 2.3–2.2 Ga, which agrees with the multistage character of metamorphism of the VCM BIF. It is postulated that more detailed investigation of high-grade BIF of the Azov Block may yield discovery of relict pyroxene with the exsolution textures similar to the ones described above. If the new data on the UHT metamorphic conditions of the BIF of the VCM reported here will be confirmed in other areas, then this suggests that the geotectonic setting of the region should be reassessed. Models of intracratonic collision between the Volgo-Uralia microcontinent and Sarmatia (Fig. 1) could explain the burial of the original sediments of the BIF to the depths required to generate the conditions of >1000 °C and 10–11 kbar found.

ACKNOWLEDGEMENTS

REFERENCES

Artemenko, G. V., 1995. Geochronological correlation of the volcanism and granitoid magmatism of the south-east part of the Ukrain shield and the Kursk magnetic anomaly. *Geochemistry and Ore Formation*, **21,** 129–154 (in Russian).

Bakker, R. J., 2003. Package FLUIDS 1. Computer programs for analysis of fluid inclusion data and for modelling bulk fluid properties. *Chemical Geology*, **194,** 3–23.

Belonoshko, A. & Saxena, S. K., 1991. A molecular dynamics study of pressure-volume-temperature properties of supercritical fluids: 2. CO_2, CH_4, CO, O_2, and H_2. *Geochimica et Cosmochimica Acta*, **55,** 3191–3208.

Bogdanova, S. V., Pashkevich, I. K., Gorbatschev, R. & Orlyuk, M. I., 1996. Riphean rifting and major Palaeoproterozoic crustal boundaries in the basement of the East European Craton: geology and geophysics. *Tectonophysics*, **268,** 1–21.

Bonnichsen, B., 1969. Metamorphic pyroxenes and amphiboles in the Biwabik iron formation, Dunka River area, Minnesota. *Mineralogical Society of America Special Paper*, **2,** 217–239.

Devaraju, T. C. & Laajoki, K., 1986. Mineralogy and mineral chemistry of the manganese-poor and manganiferous iron-formations from the high-grade metamorphic terrain of Southern Karnataka, India. *Journal Geological Society of India*, **28,** 134–164.

Duan, Z., Moller, N. & Weare, J. H., 1992. Molecular dynamics simulation of PVT properties of geological fluids and a general equation of state of nonpolar and weakly polar gases up to 2000 K and 20,000 bar. *Geochimica et Cosmochimica Acta*, **56,** 3839–3845.

Duan, Z., Moller, N. & Weare, J. H., 1996. A general equation of state for supercritical fluid mixtures and molecular dynamics simulation of mixture *PVTX* properties. *Geochimica et Cosmochimica Acta*, **60,** 1209–1216.

Fonarev, V. I., 1987. *Mineral Equilibria in the Pre-Cambrian Iron Formations (Experiment, Thermodynamics and Petrology).* Nauka, Moscow, 296 p. (in Russian).

Fonarev, V. I. & Graphchikov, A. A., 1982. Experimental study of Fe-Mg- and Ca-distribution between coexisting ortho- and clinopyroxenes at $P = 294$ MPa, $T = 750$ and 800 °C. *Contributions to Mineralogy and Petrology*, **79,** 311–318.

Fonarev, V. I. & Graphchikov, A. A., 1991. Two-pyroxene thermometry: a critical evaluation. In: *Progress in Metamorphic and Magmatic Petrology. A Memorial Volume in Honor of D.S. Korzhinsky* (ed. Perchuk, L. L.), pp. 65–92. Cambridge University Press, Cambridge.

Fonarev, V. I., Touret, J. L. R. & Kotelnikova, Z. A., 1998. Fluid inclusions in rock from the Central Kola granulit area (Baltic shield). *European Journal of Mineralogy*, **10,** 1181–1200.

Fonarev, V. I., Santosh, M., Vasiukova, O. V. & Filimonov, M. B., 2003. Fluid evolution and exhumation path of the Trivandrum Granulite Block, southern India. *Contributions to Mineralogy and Petrology*, **145,** 339–354.

Gole, M. I. & Klein, C., 1981. High-grade metamorphic Archean banded iron-formations, Western Australia: assemblages with coexisting pyroxenes ± fayalite. *American Mineralogist*, **66,** 87–99.

Gorbatschev, R. & Bogdanova, S., 1993. Frontiers in the Baltic Shield. *Precambrian Research*, **64,** 3–22.

Harley, S. L., 1985. Garnet-orthopyroxene bearing granulites from Enderby Land, Antarctica: metamorphic pressure-temperature-time evolution of the Archean Napier Complex. *Journal of Petrology*, **26,** 819–856.

Harley, S. L., 1987. A pyroxene-bearing metaironstone and other pyroxene granulites from Tonagh Island, Enderby Land, Antarctica: further evidence for very high temperature (>980 °C) Archean regional metamorphism in the Napier Complex. *Journal of Metamorphic Geology*, **5,** 341–356.

Harris, N. B. W. & Jayaram, S., 1982. Metamorphism of cordierite gneisses from the Bangalore region of the Indian Archean. *Lithos*, **15,** 89–98.

Kretz, R., 1983. Symbols for rock-forming minerals. *American Mineralogist*, **68,** 277–279.

Krogh, E. J., 1977. Origin metamorphism of iron formations and associated rocks, Lofoten-Vesteralen, N. Norway. I. The Vestpolltind Fe-Mn deposit. *Lithos*, **10,** 243–255.

Lindsley, D. H., 1983. Pyroxene thermometry. *American Mineralogist*, **68,** 477–493.

Maaskant, P., 2004. Thermobarometry of the Furua granulites, Tanzania: a comparative study. *Neues Jahrbuch für Mineralogie, Abhandlungen*, **180,** 65–100.

Mahabaleswar, B., 1986. Mineral chemistry of the silicate mineral phases of Banded Iron-Formation of high-grade region, Karnataka. *Journal Geological Society of India*, **28,** 165–178.

Sandiford, M. & Powell, R., 1986. Pyroxene exsolution in granulites from Fyfe Hills, Enderby Land, Antarctica: evidence for 1000 °C metamorphic temperatures in Archean continental crust. *American Mineralogist*, **71,** 946–954.

Savko, K. A., 1999a. Physicochemical parameters of metamorphism of eulysites from the central part of the Voronezh Crystalline Massif. Proceedings of Voronezh State University, *Geology*, **8,** 73–81 (in Russian).

Savko, K. A., 1999b. Petrology and metamorphic evolution of basic granulites of the Voronezh Crystalline Massif. Proceedings of Voronezh State University, *Geology*, **7,** 107–119 (in Russian).

Savko, K. A., 2000. Reaction textures and metamorphic evolution of spinel granulites in the Voronezh Crystalline Massif. *Petrology*, **8,** 145–160.

Shcherbak, N. P., Bartnitsky, Ye. N., Bibikova, E. V. & Boyko, V. L., 1984. Age and evolution of the Early Precambrian continental crust. In: *Archean Geochemistry: The Origin and Evolution of the Archean Continental Crust* (ed. Kröner, A.), pp. 251–261. Springer, Berlin.

Shcherbak, N. P., Artemenko, G. V. & Bartnitsky, Ye. N., 1993. Ages of the banded iron formations in the Ukrainian Shield. In: *Isotopic Dating of the Endogeneous ore Formations* (ed. Bibikova, E. V.), pp. 14–26 Nauka, Moscow (in Russian).

Shchipansky, A. A. & Bogdanova, S. V., 1996. The Sarmatian crustal segment: Precambrian correlation between the Voronezh Massif and the Ukrainian Shield across the Dniepr-Donets Aulacogen. *Tectonophysics*, **268,** 109–125.

Span, R. & Wagner, W., 1996. A new equation of state for carbon dioxide covering the fluid region from the triple-point temperature to 1100 K at pressures up to 800 MPa. *Journal of Physical Chemistry Reference Data*, **25,** 1509–1596.

Touret, J. L. R., 1981. Fluid inclusion in high grade metamorphic rocks. In: *Short Course in Fluid Inclusions: Application to Petrology* (eds Hollister, L. S. & Grafword, M. L.), pp. 182–208. Mineralogical Association of Canada, Calgary.

Vaniman, D. T., Papike, J. J. & Labotka, T., 1980. Contact metamorphic effect of the Stillwater Complex, Montana: the concordant iron formation. *American Mineralogist*, **65,** 1087–1102.

Zhai, M. & Windley, B. F., 1990. The Archean and Early Proterozoic banded iron formations of North China: their characteristics, geotectonic relations, chemistry and implications for crustal growth. *Precambrian Research*, **48,** 267–286.